A COMPARATIVE STUDY ON THE EFFECT OF MULTI-MACHINE MANUFACTURING ON ADDITIVELY MANUFACTURED PART QUALITIES

Yogesh Rajpal, Sinéad M. Uí Mhurchadha, Paul Quinn, Ramesh Raghavendra

South Eastern Applied Materials (SEAM) Research Centre, Waterford Institute of Technology, Waterford, Ireland
X91TX03

Corresponding author: Ramesh Raghavendra, rraghavendra@wit.ie

Abstract: This paper presents a comparative study on the effect of multi-machine laser powder bed fusion manufacturing on the quality of 316L stainless steel parts. Within industry, often the same additive manufacturing machines are used for research and development of components as are used for production. However, there is a challenge in terms of determining how the machine set-up and resulting part quality from one machine translates to another machine. This work determines the effect of varying machines and operators on the resultant part qualities. A build plate with specimens designed for the quantification of key material parameters was designed and manufactured on three different EOS M280 machines at different locations. This research shows the requirement to develop optimised part parameters for each AM machine and also the requirement for the standardisation of powder bed packing, which directly affect the build quality.

Key words: Additive manufacturing, Cross-site manufacturing, 316L stainless steel, Process Quality, AM Product Development, metrology.

1. INTRODUCTION

Additive Manufacturing (AM) is a fast-developing manufacturing technology that has evolved from a rapid prototyping tool to a production technology and is playing a key role in Industry 4.0 by enhancing competitiveness, as well as creating new manufacturing trends (Zhai *et al.*, 2014; Dilberoglu *et al.*, 2017). AM refers to bottom-up methods of manufacturing through a layer-by-layer deposition of material. AM expands the design space for the complex objects (Diegel *et al.*, 2019; Chantzis *et al.*, 2021), enabling exploration of new material properties, optimisation of components and parts (Kugaevskii *et al.*, 2019); thus, it is projected to disrupt supply chains for many manufacturing industries. Laser powder bed fusion (L-PBF) is one of the most commonly used metal AM techniques in highly regulated industries, such as the biomedical device industry. L-PBF systems, shown in Figure1, produce parts by distributing metal powder across build plate and selectively melting the required area

as defined by a 3D CAD design, converted into 2D slice format. The build platform is then lowered by one layer-height and a new layer of powder is deposited on the build plate by a re-coater blade. The process repeats layer-by layer until part is complete.
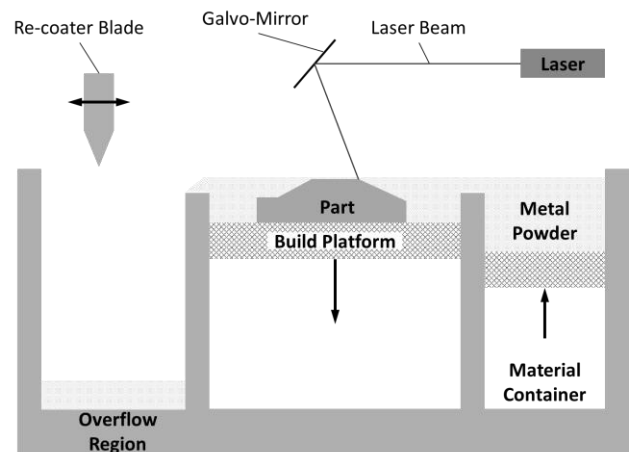

Fig. 1 Schematic diagram of L-PBF Process (image courtesy of Quinn *et al.* (2019a))

Mahesh *et al.*(2002) described benchmarking as a process to identify the "highest standards of excellence for products, services, and processes". Benchmarking is a known methodology to assess the capabilities and limitations of a process, in this case, the L-PBF AM process. It also identifies optimisation approaches and other manufacturing and process information. Mahesh *et al.*(2005) also proposed a classification for benchmarking of AM processes, depending on the purpose. These were divided into three groups:
- Geometrical benchmark: to evaluate and compare the geometrical and dimensional accuracy of the AM parts.
- Mechanical benchmark: a standard design of components to analyse and compare the AM parts mechanical properties such as ultimate tensile strength, shrinkage and creep properties.
- Process benchmark: This covers all the

benchmarking artefacts which are used to optimize the process, for example, to define the optimised process parameters for a given material or product.

With the increasing application of AM, many L-PBF systems have been developed and are available in the market for the manufacturing industry, each with its strengths and limitations. Moshiri *et al.*(2019) conducted an extensive benchmarking of L-PBF machines across five top machine producers and two end users. They designed an artefact for the study that was manufactured using maraging steel grade 300. It was found that user experience and expertise heavily influenced the final quality of product.

Within industry, companies typically have machines dedicated to research and development or production. To allow for translation of the research to the production of parts, many companies choose to use the same machines throughout their research and manufacturing facilities. Therefore, there is a challenge in terms of determining how the machine set-up and resulting part quality from one machine translates to another machine by the same manufacturer. Furthermore, often as a company expands their AM facilities to increase production capacity, they must understand how part qualities differ from machine-to-machine.

This research presents a comparative study into the effect of multi-machine manufacturing using standard parameters and 316L powder from a single batch, on the resulting part qualities. A build plate with specimens designed for the quantification of key material parameters, such as surface roughness, part density, dimensional accuracy, residual stress and mechanical properties, was designed and printed on three different EOS M280 L-PBF machines in different locations. The effect of powder packing on the build qualities was also investigated by inducing an unevenly packed powder bed within the process. This research characterises the effect of multi-machine-multi-operator set-up on resultant part qualities. This is of direct relevance to modern manufacturing in a research and development and production environment.

2. METHODS AND MATERIALS

2.1 Manufacturing layout and set-up

A build plate of investigative parts was designed to capture different part qualities. The part qualities investigated have been identified as critical qualities for AM parts as per ISO 17296 (ISO/TC 261 Additive manufacturing, 2015). This research focuses on four of these properties as follows (see Table 1):

- Build material requirements: density and microstructure analysis.
- Geometric requirements: dimensional and geometrical tolerance.
- Surface requirements: surface roughness.
- Mechanical requirements: hardness and tensile strength.
- L-PBF Process requirements: powder distribution and packing on the build plate.

The build plate layout and parts are presented in Figure 2. This build file was manufactured in three locations (Sites A, B and C) on EOS M280 machines using the same machine parameters. This allows for the investigation of the effect of multi-machine manufacturing, including cross-site manufacturing and multiple operators, on the quality of parts produced using L-PBF.

In this study, parts were manufactured using gas-atomized 316L stainless steel virgin powder supplied by LPW Technology Ltd. (now Carpenter Additive) (*Technical Data Sheet CT PowerRange 316L F*, 2019). The powder used in all three manufacturing sites was from a common powder batch. The purpose of using virgin powder from the same batch was to avoid any effects of recycled powder (P. Quinn *et al.*, 2019b) or differences between powder batches that could influence the results of this study (Sun *et al.*, 2018). A common build file was developed at Site A, to be used across the remaining manufacturing sites. This file ensured that the same build file, part layout and laser parameters were used for the entire study. The laser calibration records for each manufacturing site were also requested to ensure all machines were sufficiently calibrated. This procedure was selected in order to replicate multiple machine manufacturing within an industrial setting. This procedure ensured that the only variable that was unknown in the study was the initial operator set-up. Once manufactured all parts were removed from the build plate using Wire Electric Discharge Machining and tested at Site A.
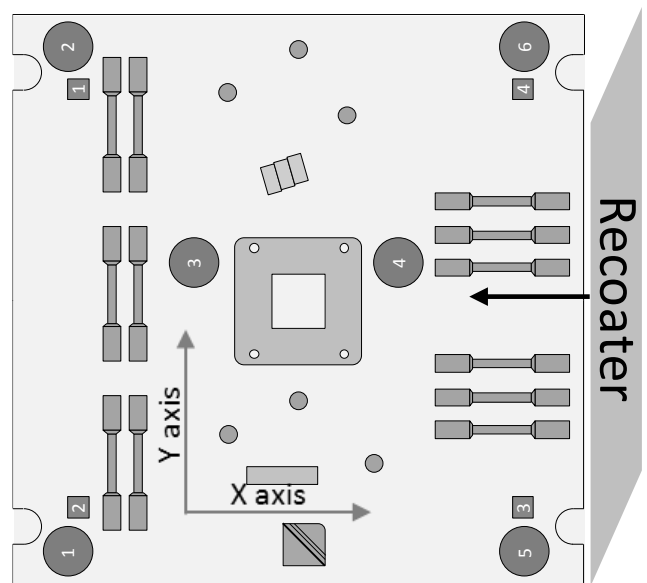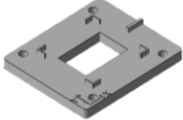

Fig. 2. Build Plate Layout

Table 1. Test Summary

Part Characteristics	Test method	Part
Density	Cross-sectional analysis	Density Cube
Microstructure	Cross-sectional analysis	Density Cube
Part dimensional accuracy	Coordinate measurement	Calibration Plate
Feature dimensional accuracy	SEM Imaging and image analysis	Geometry Block
Surface roughness	White light interferometry	Overhang
Hardness	Zwick Roell Rockwell hardness testing	Geometry Block
Residual Stress	Deformation measurement	Arch
Tensile Strength	Tensile testing	Tensile specimen
Powder distribution during manufacturing	Gas pycnometry	Powder Capsule

2.2 Characterisation methods
Part density and microstructural analysis
Sample density was calculated in terms of the porosity within the build part. For porosity measurements, cubes were built in the four corners of each build plate (see Figure 2). These cubes were ground and polished to reveal the internal bulk material. A Keyence Digital Microscope at x200 magnification was used to image five locations on the cube. The percentage porosity was calculated using image manipulation in ImageJ (Schneider *et al.*, 2012). The average density from five measurements was used for part density measurements.

Furthermore, the microstructural inspection was done on the same specimens by etching with Fry's reagent for 60 to 90 seconds. The etched surfaces were imaged using a Keyence Digital Microscope at x200 magnification.

Dimensional accuracy
A calibration plate (as shown in Figure 3) is a standard part designed by EOS (EOS Gmbh, 2014) to test the laser accuracy of the machine. This part was printed to investigate the differences between laser histories at the different manufacturing sites. During the life of each printer, the output power of the laser and laser beam focus will change, as the accumulated laser exposure hours increase. The laser power will affect the curing zone of the laser and thus, the required laser scaling and offset for the machine. These changes can be tracked during the servicing of the printer and can be adjusted via laser offset and scaling parameters. To allow for direct comparison between build sites in this study, each manufacturer used the same values for these parameters. The calibration plate used to measure the differences between the M280 laser offset and scaling for each manufacturing site is presented in Figure 3.
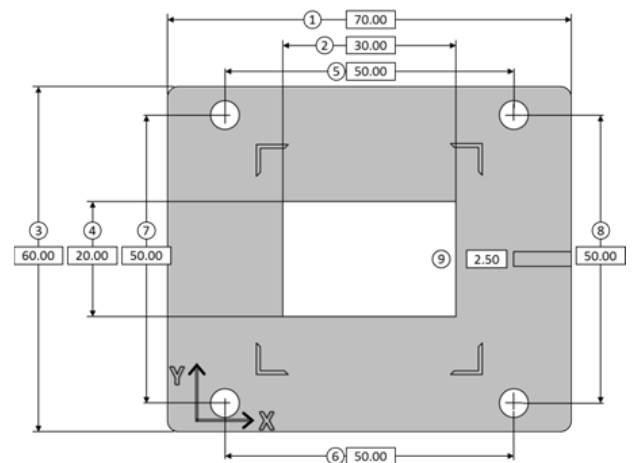

Fig. 3. Calibration plate with nominal dimensions

A QVI Smartscope CNC 500, with a dimensional resolution of approximately 0.5 µm, was used to measure the dimensions of the calibration plate, as shown in Figure 3 before the parts were removed from the build plate. This ensured the plate was measured in its as built state. Using these measurements, the scaling factor and the offset in the laser beam were calculated. The scaling factor for dimensional accuracy represents the deviation of the actual manufactured length from the nominal design length of a part. A zero-scaling factor result would represent the machine producing the nominal dimension. Positive scaling factor shows that the as-built dimension was less than the nominal dimension for the part; similarly, a negative scaling factor indicates that the actual dimension was bigger than nominal dimension. The scaling factor was calculated using the dimension of the distance between the holes centre, as follows:

$$\text{Scaling Factor} = ((\text{Nominal length})/(\text{Actual length}))*100-100 \qquad (1)$$

where the nominal length was the designed (CAD) length, and the actual length was as measured. The

distance between the centres of the holes was used as there would be no effect on the centre of the hole due to any laser deviation. The scaling factor was found using dimensions 5, 6, 7, and 8 in Figure 3 and averaged for the x- and y-directions. The nominal deviation was calculated using dimensions 1, 2, 3, and 4 using the calculated scaling factor, as follows:

$$\text{Nominal Deviation} = (\text{Actual length }(100+ \text{Scaling Factor}))/100 \qquad (2)$$

The beam deviation (or beam offset) can be defined as the deviation of the laser from its nominal scan path. This beam deviation can be used to calibrate the laser by correcting the beam offset value. The beam deviation for each site was calculated using equation (3), below. The average beam deviation for dimensions 5 to 8 was compared between the different sites.

$$\text{Beam Deviation} = ((\text{Nominal Deviation} - \text{Nominal length}))/2 \qquad (3)$$

Furthermore, a geometry block was printed and inspected to measure the accuracy of the machine in terms of manufacturing features, such as slots and the the circularity of a hole built in the z-direction. The measurements of the slots were completed using Scanning Electron Microscopy (SEM) imaging at x500 magnification. For the circularity of the hole, images were taken using a Smartscope CNC 500 at x32.5 and circularity was calculated through image analysis using ImageJ software (Schneider et al., 2012). The circularity, C, of the hole is given by:

$$C=4\pi(A/P^2) \qquad (4)$$

where A is the area of the hole and P is the perimeter of the hole. A circularity value of 1 depicts a perfectly circular hole (Cox, 1927).

Surface roughness
Surface roughness was measured using Bruker Contour GT-K white light interferometry (WLI) with a vertical resolution of approximately 0.1 nm. This technology allows for non-contact measurement of the arithmetic mean, Ra, of the surface profile. Five measurements at x27.5 magnification of each overhanging surface were measured and averaged to provide a greater representation of the overall surface roughness.

Mechanical properties
Part hardness was measured on ground and polished surfaces of the geometry block using a Zwick Roell Rockwell hardness tester with a 1/16" ball indenter on the HRB scale in x, y and z-directions. Calibration of the instrument was confirmed using a standard

block before testing and three hardness measurements of each surface were recorded and then averaged.
Tensile specimens built in the z-direction were machined on a lathe and tested using Instron 8801 100 kN tensile testing machine at 3 mm/min crosshead speed as per the ASTM Standard (ASTM Standard E8/E8M-13a, 2013) and the recorded stress and strain data was plotted. The z direction was tested as this will provide us with the lowest tensile value for L-PBF samples (Diegel et al., 2019).
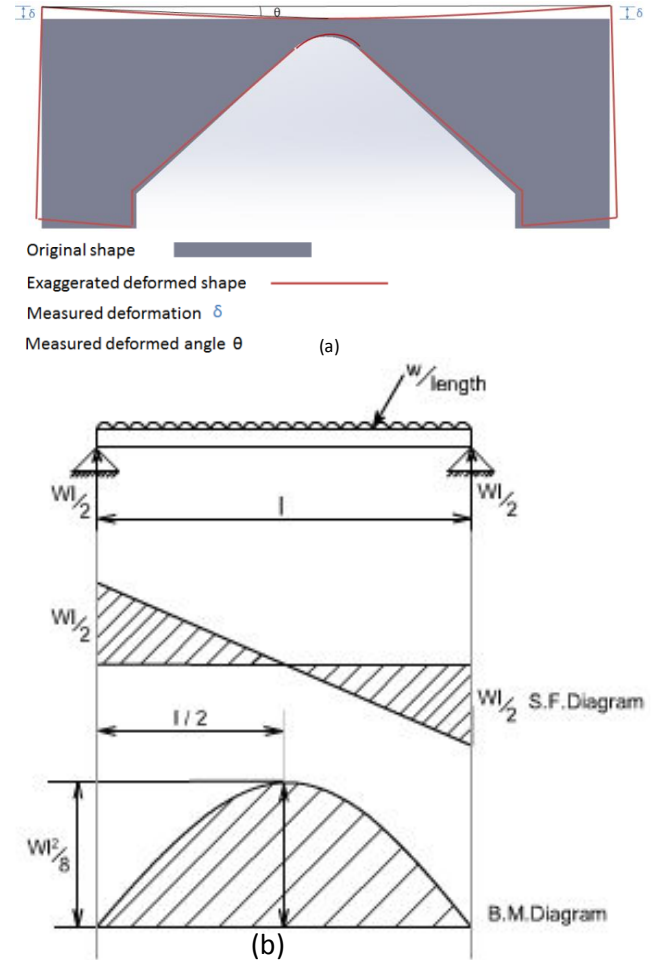

Fig. 4. (a) Exaggerated effect of residual stress on the deformation on the arch, and (b) Simply supported beam with a constant load applied and its corresponding shear force and bending moment diagrams

Residual stress measurement
Due to the thermal history of the part during the additive manufacturing process, residual stresses is generated within components, which can affect the fatigue life, corrosion resistance, crack propagation, the overall form and dimensional accuracy of parts (Li et al., 2018). To quantify residual stress from the builds an arched test piece was designed and built. After the build was completed, the arched components were removed from the plate and the distortion of the part was measured using QVI Smartscope CNC 500 at x32.5 magnification. Figure 4(a) shows an exaggerated effect of residual stress on

the arch illustrating the measured deformation, δ, at the centre of the arch. The deformation of the arch was considered to be equivalent to that of a simply supported beam under a constant load, as shown in Figure 4(b). Using beam mechanics, the residual stress associated with the deformation of the arched specimen was calculated (Hibbler, 2016) as the maximum stress, σ_R, at the centre of the arch is expressed as follows:

$$\sigma_R \approx 3200\delta/3 \qquad (5)$$

Powder distribution during manufacturing

Powder distribution across the build plate is one of the most important factors for the manufacture of consistent parts by L-PBF. Studies done by Benson and Snyders (2015) and Sutton et al. (2016) found that powder size and its distribution on build plate affect the part. In this research, the focus is on the powder distribution across the build plate using brush recoater in for the same build in different machines. To investigate this, powder capsules were placed at 6 positions across the build plate, as shown in Figure 2. The locations were chosen to be at the four extreme corners of the build plate, as well as before and after a part with a large cross-section. The location of these samples was selected in order to assess the powder deposition process in the four extremes of the build plate as well as assessing the influence of large parts on the powder distribution. The density of these capsules was measured using a Micromeritics AccuPyc Helium pycnometer.

3. RESULTS

3.1 Effect of multi-site manufacturing on part qualities

Part density and microstructural analysis

Figure 5 presents examples of the binary images at x200 magnification used to measure percentage density for each manufacturing site. Pores in the parts are shown as black specks on the solid white base metal.

Visually, parts produced at Site A are the best in terms of part densities and parts produced at Site C are the most porous. This was confirmed through image analysis of all the cross-section images of the cubes build at each manufacturing site. Therefore, there is an effect of multi-machine (or cross-site) manufacturing on the quality of the parts produced, in terms of bulk material density.

Figure 6 presents the etched micro-sections of parts build at each manufacturing site. To meet the desired microstructure, parts should have a uniform fusion of grain and should not contain any unfused powder within the microstructure. Samples from all sites were observed to have achieved the desired microstructure and did not show any abnormalities. The etched microstructures demonstrate the expected columnar grain structure in the z-direction.

Dimensional accuracy

Table 2 presents the x and y-direction scaling factors and the beam deviation for each manufacturing site as measured from the calibration plate. The results show that there is a difference in the scaling factors across all three manufacturing sites. This is due to the differences between the laser histories of each machine. Sites A and B both have positive scaling factor whereas site C scaling factor is negative, and the absolute value is larger than those of Sites A and B. Also, all sites have negative beam deviation.

Figure 7 presents SEM measurements for the slots and optical microscope images that were used for the measurement of the hole circularity. Table 3 presents the dimensions of slots of various thicknesses and hole-circularity in the z-direction of the as manufactured geometry block. For the measured dimensions of the geometry block, Site C's samples achieved more accurate build dimensions in comparison to Sites A and B, as seen by the lower deviation from the nominal dimensions.
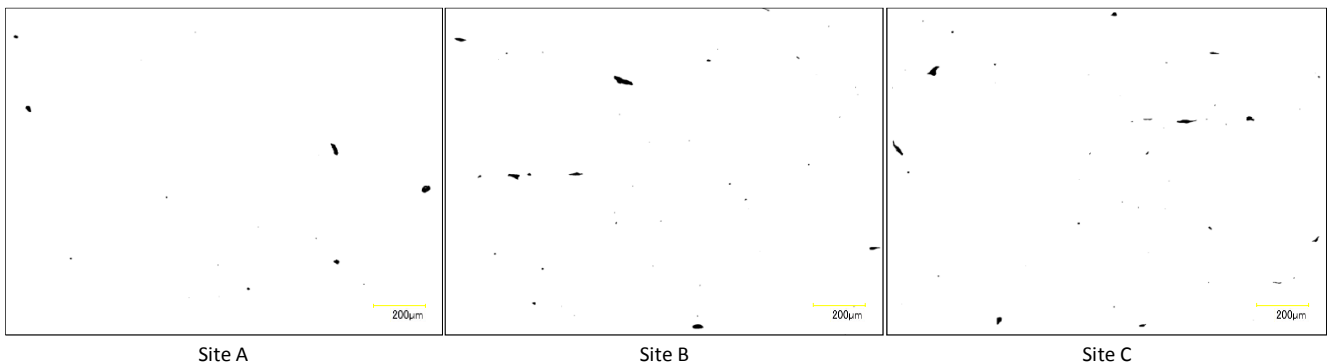

Site A   Site B   Site C

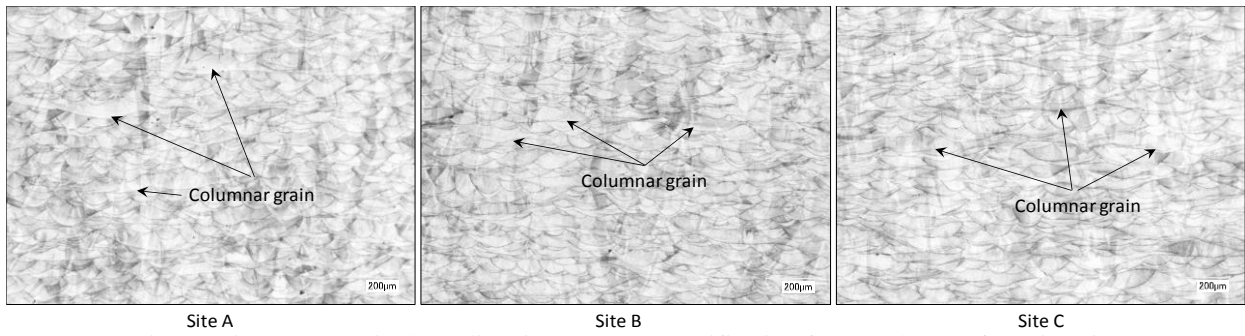Fig. 5. Example of the binary image at x200 magnification used for image analysis

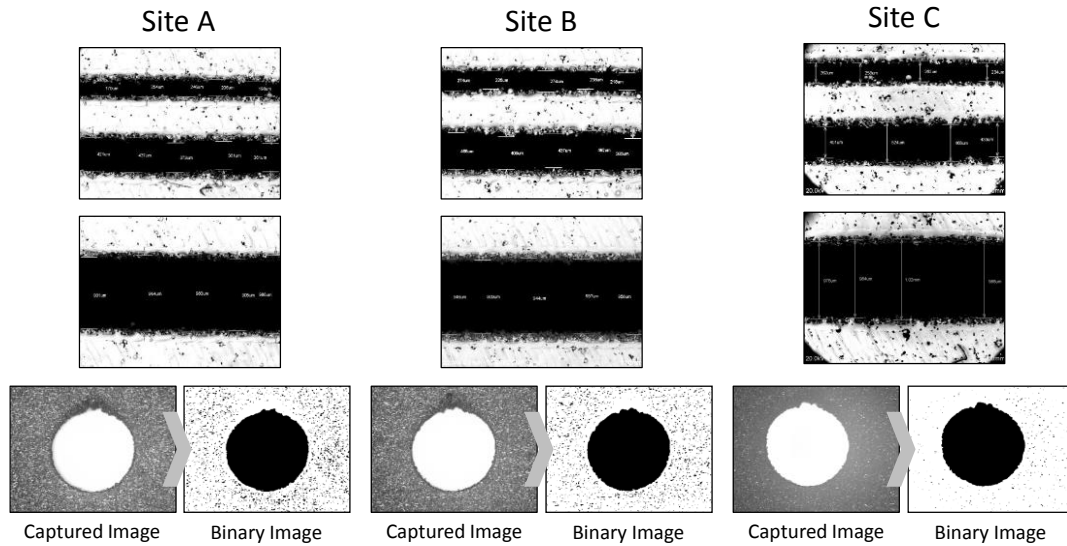Fig. 6. Microstructure in the z-direction at x200 magnification from each manufacturing site

Fig. 7. SEM measurements and image analysis for circle accuracy measurement

Table 2. Scaling factor of dimension in x and y-direction and beam deviation

Dimension Parameters	Site A	Site B	Site C
x-Scaling	0.037	0.03	-0.245
y-Scaling	0.011	0.127	-0.166
Beam deviation	-0.057	-0.076	-0.067

Table 3. Dimensions of horizontal gaps and hole-circularity

Dimension	Nominal	Site A	Site B	Site C
Gap	0.25 mm	0.19	0.23	0.25
Gap	0.50 mm	0.41	0.44	0.47
Gap	1.00 mm	0.94	0.97	0.98
Circularity (C)	1	0.75	0.79	0.75

Surface roughness

The average surface roughness measurements of the upward facing (labelled 1 to 3) and downward facing (labelled 4 to 6) surfaces for each manufacturing Sites A, B and C are presented in Table 4 with the standard error, SE, associated with each averaged measurement. Surface roughness results meet the material requirements (*EOS SS316L,* 2014), No significant difference were observed between different sites.

Table 4. Surface Roughness Measurements

| Side	Surface	Site A		Site B		Site C	
		Ra (µm)	SE	Ra (µm)	SE	Ra (µm)	SE
Up	1	11.46	0.92	9.79	0.95	13.37	1.48
	2	12.28	1.10	11.70	0.37	10.08	0.83
	3	12.45	0.93	9.89	0.77	13.34	1.12
Down	4	7.46	0.17	8.22	0.69	9.07	0.20
	5	11.17	0.71	10.48	0.56	9.52	0.36
	6	9.14	0.66	10.77	1.31	8.59	0.56

Mechanical properties

Table 5 presents the hardness data of the geometry block in different directions for each manufacturing site. The standard error, SE, associated with each averaged hardness measurement is also provided. Results meet the material standard requirement of 89 HRB for as manufactured samples (E*OS SS316L,* 2014). There is no significant difference observed between the different manufacturing sites.

Table 5. Hardness Measurement Data

Build Location	X-Direction Hardness (HRB)	Y-Direction Hardness (HRB)	Z-Direction Hardness (HRB)
Site A	95.60	94.20	93.27
Site B	95.63	94.20	94.20
Site C	94.93	93.77	92.10

The stress-strain responses in the vertical, z-direction, and horizontal, x-direction, are presented in Figure 8. The corresponding ultimate tensile strength (UTS) and elongation (%) measured by testing, *n*, number of samples are summarised in Table 6. The parts have a columnar grain structure in the z-direction, shown in Figure 6, as compared to an equiaxed grain structure expected in the x- and y-direction (Takaichi *et al.*, 2013). Hence, the AM part is found to have higher tensile strength in the x-direction (horizontal) than the z-direction (vertical), as shown in Table 6. No significant difference is observed in the elastic region and UTS across all manufactured build plates.
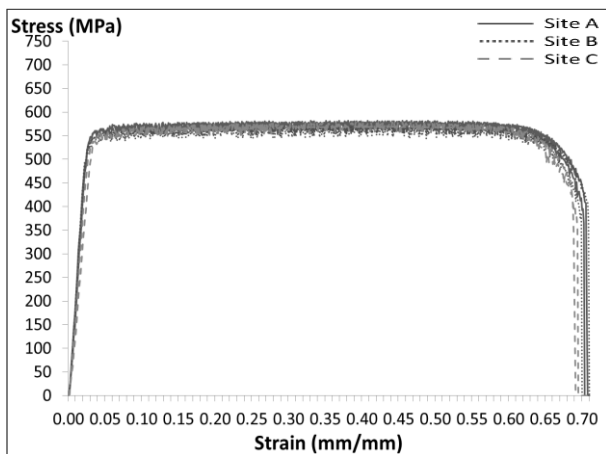
(a)
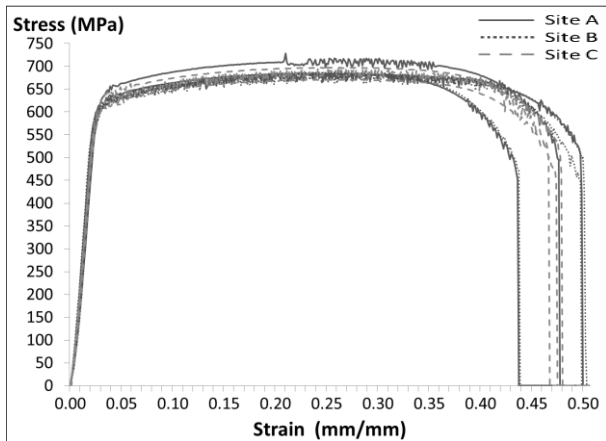
(b)

Fig. 8. Stress-strain responses for specimen build in (a) vertical (z) direction, (b) horizontal (x) direction

Table 6. Tensile test measurements

Build Location	n	Direction	UTS, MPa	SE	Elongation, %	SE
Site A	3	x	700	0.54	39	3.08
	2	z	580	0.05	62	1.80
Site B	3	x	686	0.36	40	2.93
	2	z	569	0.35	59	1.43
Site C	3	x	688	0.15	38	1.18
	2	z	577	0.14	61	0.67

Residual Stress

Table 7 presents the deformation of the residual stress arches and corresponding calculated maximum stress at the centres of the arch, for each manufacturing site. Figure 9 shows the parts visual condition. Site C has considerably more residual stress as compared to Sites A and B. Slight over-burn marks were observed in the part from Site B, more severe burn marks were also observed in the sample from site C whereas there was no burn marks evident in the sample from Site A, this is highlighted in Figure 9. The effects of residual stress can be attributed to this over-heating of the part, which results in more severe deformation and increased residual stress of the arches as shown by the result from Site C.

Table 7. Measured deformation and residual stress data in the arch from each manufacturing site

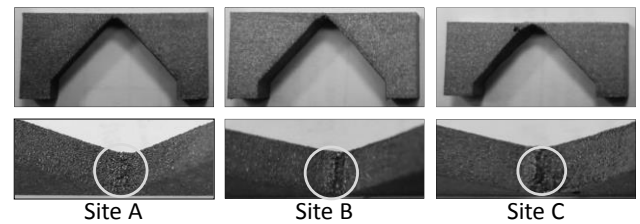| Build Location	Measured Deformation, δ [mm]	Residual Stress, σ_R [MPa]
Site A	0.096	102.22
Site B	0.104	110.61
Site C	0.158	168.04

Site A   Site B   Site C

Fig. 9. Residual stress arches highlighting burning marks on the downward surface

3.2 Effect of multi-site manufacturing on build process quality

To investigate the effect of operator set-up such as initial powder packing on the powder distribution across the build plate, the density of powder capsules was measured using a helium pycnometer and compared between each manufacturing site. During the set-up of the EOS M280, the powder is packed in the dispenser manually, and therefore, this could vary between setups and operators.

Figure 10(a) presents the density comparison of the powder capsules in the x-direction (re-coater direction), comparing the samples close to the powder dispenser (6, 4, and 5) and the samples away from the dispenser (2, 3, and 1). It is observed that the density of the samples from Site A is consistent across the build plate. Sites B and C powder capsule density decreases the further away from the powder dispenser the sample is suggesting a lack of powder being distributed in the re-coater direction. Figure 10(b) presents a density comparison of the powder

capsules in the y-direction and infers that all build samples show consistency in the density of the capsules close to the powder dispenser (samples 5 and 6). Those samples away from the powder dispenser (samples 1 and 3), show a difference in capsule density for all build sites, inferring that powder distribution is not uniform across the plate.

To further investigate this theory, an additional build plate was built at Site A in which half the powder in the dispenser was unpacked before the build, as shown in Figure 11.

Figure 12(a) presents the density comparison of the powder capsules in the x-direction built by a partially packed dispenser and a fully packed dispenser (as presented previously in Figure 10 for Site A). It is observed that in the x-direction (re-coating direction), the density of the powder capsule is lower in the unpacked region (capsules 2 and 6) in comparison to the packed region (capsules 1 and 5).

Figure 12(b) presents density comparison of the powder capsules in the y-direction and it is observed that the density of powder capsules (2 and 6) in the unpacked region is less than powder capsule in the packed region (capsules 1 and 5). Overall, there is a difference in the density of the samples built in the un-packed and the packed area. It should also be noted that capsule density in the unpacked area changed drastically further from the powder dispenser compared to the fully packed area. However, in packing half the dispenser, the unpacked half was also packed slightly due to the movement of particles in the packed section. Future work will investigate the powder distribution across build plates for fully unpacked powder versus fully packed.
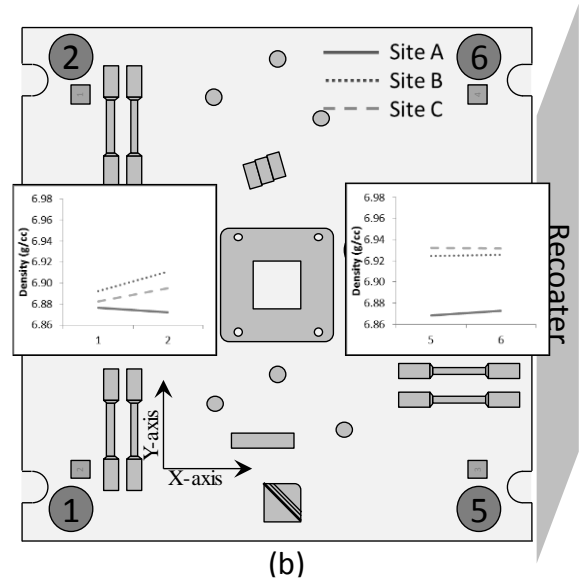

(b)

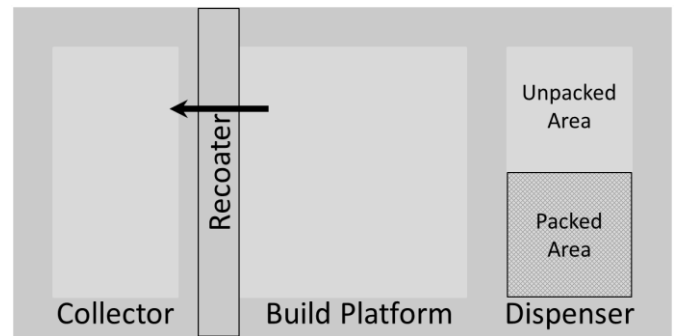Fig. 10. Comparison of percentage density achieved in (a) x-direction, (b) y-direction
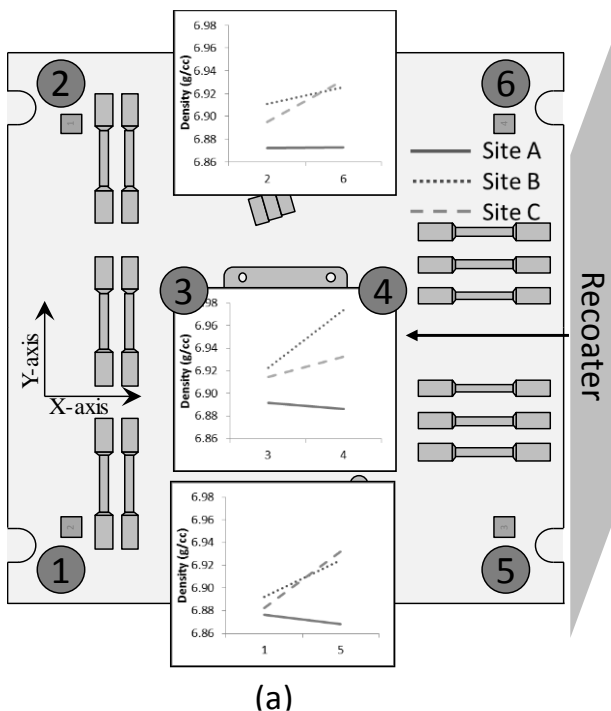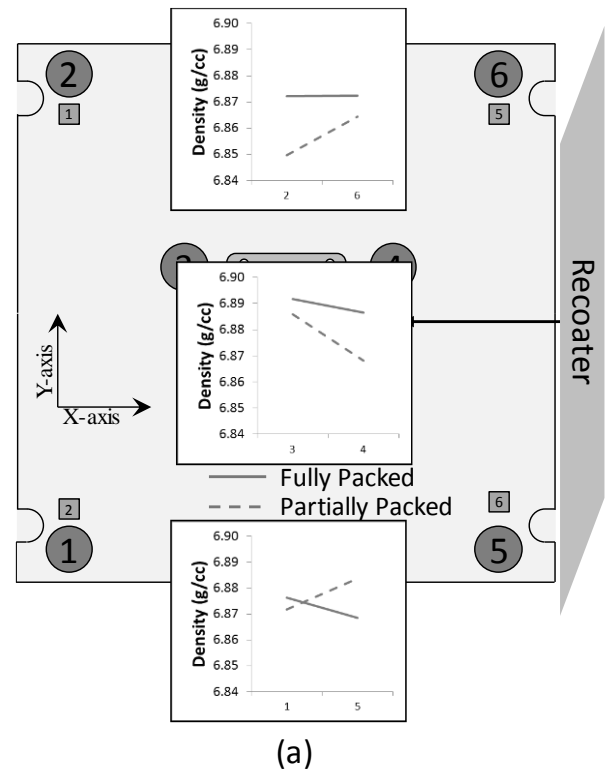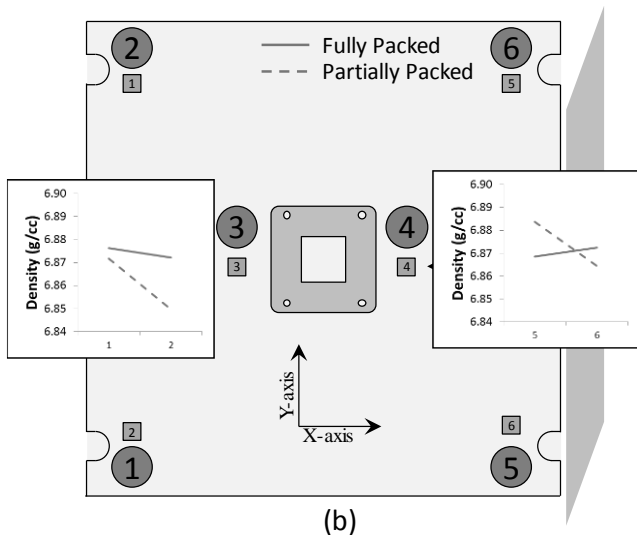

Fig. 11. Partial packed dispenser

(a)

(a)

Fig. 12. Density comparison of fully packed and partially packed powder capsules across (a) x-direction, and (b) y-direction

4. CONCLUSIONS

The effect of cross-site L-PBF manufacturing on the resulting part qualities has been investigated in this paper. This study has identified an area to consider in mass production of the AM parts which can affect many industries. Various test samples were identified to measure key part qualities, viz. dimensional accuracy, porosity, mechanical strength, surface roughness, residual stress and powder distribution. The effect of multi-site manufacturing on part qualities and build process qualities are as follows:

- **Effect of multi-site manufacturing on part qualities**: The use of machines with different laser histories, effects the individual machine laser focus and performance, this results in differences in part accuracy. Therefore, separate laser focus calibrations must be conducted on each machine at regular intervals to ensure the correct laser focus can be applied to the build.

- **Effect of multi-site manufacturing on build process quality:** There is an operator set-up effect in the EOS M280 machine that is noticeable in terms of powder distribution across the build plate during the recoating process. A standard procedure for the initial set-up of the machine, with a standardised method to pack the powder for all operators is necessary to eliminate the effect of the operator on the resulting manufactured sample quality.

5. ACKNOWLEDGEMENTS

6. REFERENCES

1. ASTM Standard E8/E8M-13a, (2013). *Standard Test Methods for Tension Testing of Metallic Materials'*, ASTM International, doi: 10.1520/E0008_E0008M-13A.

2. Benson, J. M. and Snyders, E. (2015). *The need for powder characterisation in the additive manufacturing industry and the establishment of a national facility*, The South African Journal of Industrial Engineering, **26**(2), p.104, doi: 10.7166/26-2-951.

3. Chantzis, D., Liu, X., Politis, D. J., Shi, Z. and Wang, L. (2021). *Design for additive manufacturing (DfAM) of hot stamping dies with improved cooling performance under cyclic loading conditions*, Additive Manufacturing. Elsevier B.V., **37**, p. 101720. doi: 10.1016/j.addma.2020.101720.

4. Cox, E. P. (1927). *A Method of Assigning Numerical and Percentage Values to the Degree of Roundness of Sand Grains*, Journal of Paleontology, **1**(3), pp. 179–183. Available at: https://www.jstor.org/stable/1298056?seq=1#metadata_info_tab_contents, accessed on: 12 January 2021

5. Diegel, O., Nordin, A. and Motte, D. (2019). *A Practical Guide to Design for Additive Manufacturing*. Singapore: Springer Singapore (Springer Series in Advanced Manufacturing). doi: 10.1007/978-981-13-8281-9.

6. Dilberoglu, U. M., Gharehpapagh, B., Yaman, U. and Dolen, M. (2017). *The Role of Additive Manufacturing in the Era of Industry 4.0*, Procedia Manufacturing. Elsevier B.V., **11**, pp. 545–554. doi: 10.1016/j.promfg.2017.07.148.

7. EOS Gmbh, (2014). *EOSINT M280 Training Manual (Basic Training)*, pp. 9.1-9.4.

8. Hibbler, R. C. (2016). *Mechanics of Materials*. 10th editi. Pearson Education (US). Available at: https://www.bookdepository.com/Mechanics-Materials-Russell-C-Hibbeler/9780134319650, accessed on: 12 January 2021.

9. ISO/TC 261 Additive manufacturing (2015). *ISO 17296-2 Additive manufacturing — General principles — Overview of process categories and feedstock*, ISO, Geneva, Switzerland, p. 8.

10. Kugaevskii, S., Pizhenkov, E. and Gamberg, A. (2019). *The effectiveness of additive SLM-technologies in the manufacture of cutting tools*, Materials Today: Proceedings, **19**(Part 5), pp. 1977–1981. doi: 10.1016/j.matpr.2019.07.055.

11. Li, C., Liu, Z. Y., Fang, X. Y. and Guo, Y. B. (2018). *Residual Stress in Metal Additive Manufacturing*, Procedia CIRP, **71**, pp. 348–353. doi: 10.1016/j.procir.2018.05.039.

12. Mahesh, M., Wong, Y. S., Fuh, Y. H. and Loh, H. T. (2002). *Rapid prototyping and manufacturing benchmarking*, Sofwtare Solutions for RP.

13. Mahesh, M., Fuh, J. Y. H., Wong, Y. S. and Loh, H. T. (2005). *Benchmarking for decision making in rapid prototyping systems*, in *I*EEE International Conference on Automation Science and Engineering, IEEE, pp. 19–24. doi: 10.1109/COASE.2005.1506739.

14. *Material data sheet EOS StainlessSteel 316L for EOS M 280* (2014). *EOS GmbH - Electro Optical Systems*. Available at: https://cdn1.scrvt.com/eos/77d285f20ed6ae89/dd6850c010d3/EOSStainlessSteel 316L.pdf, accessed on: 12 January 2021.

15. Moshiri, M., Candeo, S., Carmignato, S. and Mohanty, S. (2019). *Benchmarking of Laser Powder Bed Fusion Machines*. doi: 10.3390/jmmp3040085.

16. Quinn, Paul, Halloran, S. O., Ryan, C., Pamell, A., Lawlor, J. and Raghavendra, R. (2019a). *Development of a standalone in-situ monitoring system for defect detection in the direct metal laser sintering process*, in An Additive Manufacturing Conference, pp. 1390–1399. Available at: http://utw10945.utweb.utexas.edu/sites/default/files/2 019/120 Development of a Standalone In-Situ Monitoring Sys.pdf.

17. Quinn, P., O'Halloran, S., Lawlor, J. and Raghavendra, R. (2019b). *The effect of metal EOS 316L stainless steel additive manufacturing powder recycling on part characteristics and powder reusability*, Advances in Materials and Processing Technologies. Taylor & Francis, **5**(2), pp. 348–359. doi: 10.1080/2374068X.2019.1594602.

18. Schneider, C. A., Rasband, W. S. and Eliceiri, K. W. (2012). *NIH Image to ImageJ: 25 years of image analysis*, Nature Methods, **9**(7), pp. 671–675. doi: 10.1038/nmeth.2089.

19. Sun, Y., Aindow, M. and Hebert, R. J. (2018). *Comparison of virgin Ti-6Al-4V powders for additive manufacturing*, Additive Manufacturing. Elsevier, 21(February), pp. 544–555. doi: 10.1016/j.addma.2018.02.011.

20. Sutton, A. T., Kriewall, C. S., Leu, M. C. and Newkirk, J. W. (2016). *Powder characterisation techniques and effects of powder characteristics on part properties in powder-bed fusion processes*, Virtual and Physical Prototyping, **12**(1), pp. 3–29. doi: 10.1080/17452759.2016.1250605.

21. Takaichi, A., Suyalatu, Nakamoto, T., Joko, N., Nomura, N., Tsutsumi, Y., Migita, S., Doi, H., Kurosu, S., Chiba, A., Wakabayashi, N., Igarashi, Y. and Hanawa, T. (2013). *Microstructures and mechanical properties of Co–29Cr–6Mo alloy fabricated by selective laser melting process for dental applications,* Journal of the Mechanical Behavior of Biomedical Materials, **21**, pp. 67–76. doi: 10.1016/j.jmbbm.2013.01.021.

22. *Technical Data Sheet CT PowerRange 316L F* (2019). *Carpenter Additive*. Available at: https://www.carpenteradditive.com/hubfs/carpenter_a dditive/image/Resources/Datasheets/CT PowerRange 316L F.pdf, accessed on: 12 January 2021.

23. Zhai, Y., Lados, D. A. and LaGoy, J. L. (2014). *Additive Manufacturing: Making Imagination the Major Limitation*, JOM, **66**(5), pp. 808–816. doi: 10.1007/s11837-014-0886-2.